01 Feb 2011

Study Of Emission Turbulence-radiation Interaction In Hypersonic Boundary Layers

L. (Lian) Duan
Missouri Unviersity of Science and Technology, duanl@mst.edu

M. P. Martín

I. Sohn

D. A. Levin

et. al. For a complete list of authors, see https://scholarsmine.mst.edu/mec_aereng_facwork/5450

Recommended Citation

L. Duan et al., "Study Of Emission Turbulence-radiation Interaction In Hypersonic Boundary Layers," *AIAA Journal*, vol. 49, no. 2, pp. 340 - 348, American Institute of Aeronautics and Astronautics, Feb 2011.
The definitive version is available at https://doi.org/10.2514/1.J050508

AIAA JOURNAL
Vol. 49, No. 2, February 2011

Study of Emission Turbulence–Radiation Interaction in Hypersonic Boundary Layers

L. Duan* and M. P. Martín†
University of Maryland, College Park, Maryland 20742
I. Sohn‡ and D. A. Levin§
Pennsylvania State University, University Park, Pennsylvania 16802
and
M. F. Modest¶
University of California, Merced, Merced, California 95344

DOI: 10.2514/1.J050508

Direct numerical simulations are conducted to study the effects of emission turbulence–radiation interaction in hypersonic turbulent boundary layers, representative of the Orion Crew Exploration Vehicle at peak-heating condition during reentry. A nondimensional governing parameter to measure the significance of emission turbulence–radiation interaction is proposed, and the direct numerical simulation fields with and without emission coupling are used to assess emission turbulence–radiation interaction. Both the uncoupled and coupled results show that there is no sizable interaction between turbulence and emission at the hypersonic environment under investigation. An explanation of why the intensity of emission turbulence–radiation interaction in the hypersonic boundary layer is smaller than that in many combustion flows is provided.

Nomenclature

B	=	Einstein absorption coefficient
E	=	total energy, $\sum_s^{ns} \rho_s(e_s + \frac{1}{2}u_i u_i)$, J/m^3
g	=	electronic state degeneracy
H	=	shape factor, δ^*/θ, dimensionless
h	=	specific enthalpy, J/kg
h	=	Planck's constant
h°	=	enthalpy of formation, J/kg
I_λ	=	radiative intensity, W/cm^2-μ-sr
J	=	diffusive mass flux, kg/m$^2 \cdot$ s
Le	=	Lewis number, dimensionless
M	=	Mach number, dimensionless
n	=	number density, m^{-3}
p	=	pressure, $\sum_s \rho_s(\hat{R}/M_s)T$, Pa
q	=	heat flux, J/(m$^2 \cdot$ s)
q	=	turbulence kinetic energy, $(u'^2 + v'^2 + w'^2)/2$, m^2/s^2
q_C	=	conductive heat flux, $-\kappa(\partial T/\partial x_j)$, J/(m$^2 \cdot$ s)
q_R	=	radiative heat flux, J/(m$^2 \cdot$ s)
$Re_{\delta 2}$	=	Reynolds number, $\equiv \rho_\delta u_\delta \theta/\mu_w$, dimensionless
Re_θ	=	Reynolds number, $\equiv \rho_\delta u_\delta \theta/\mu_\delta$, dimensionless
Re_τ	=	Reynolds number, $\equiv \rho_w u_\tau \delta/\mu_w$, dimensionless
S_{ij}	=	strain rate tensor, $\frac{1}{2}(\partial u_i/\partial x_j + \partial u_j/\partial x_i)$, s^{-1}
T	=	translational temperature or temperature in general, K
T_e	=	electron temperature, K
T_r	=	rotational temperature, K
T_v	=	vibrational temperature, K
u	=	velocity, m/s
u_τ	=	friction velocity, m/s
δ	=	boundary-layer thickness, mm
δ^*	=	displacement thickness, mm
ε	=	emission coefficient, W/cm^2-μ-sr
ε	=	total emission, W/cm^3
ε	=	dissipation rate, m^2/s^3
θ	=	momentum thickness, mm
κ	=	absorption coefficient, cm^{-1}
κ	=	mixture thermal conductivity, J/(K $\cdot$ m $\cdot$ s)
λ	=	wavelength, Å
μ	=	mixture viscosity, kg/(m $\cdot$ s)
ρ	=	density, kg/m^3
σ_{ij}	=	shear stress tensor, $2\mu S_{ij} - \frac{2}{3}\mu\delta_{ij}S_{kk}$, Pa

Subscripts

b	=	blackbody value
L	=	lower state
s	=	chemical species
U	=	upper state
δ	=	boundary-layer edge
λ	=	at a given wavelength

Superscripts

$+$	=	inner-wall units
$*$	=	normalized quantity

Presented as Paper 2010-0354 at the 48th AIAA Aerospace Sciences Meeting, Orlando, FL, 4–7 January 2010; received 18 February 2010; revision received 27 October 2010; accepted for publication 1 November 2010.

*Visiting Graduate Student, Department of Aerospace Engineering. Student Member AIAA.
†Graduate Student, Department of Aerospace Engineering. Student Member AIAA.
‡Associate Professor, Department of Aerospace Engineering. Senior Member AIAA.
§Professor, Department of Aerospace Engineering. Associate Fellow AIAA.
¶Shaffer and George Professor of Engineering, School of Engineering. Associate Fellow AIAA.

I. Introduction

THERMAL radiation has long been recognized to contribute significantly to the overall heat load [1] for spacecraft during entry into planetary atmospheres or Earth return, which typically has velocities exceeding 10 km/s. The radiative heat load onto such vehicles comes from both the radiation within the boundary layer, as well as the transmission of external radiation hitting the boundary layer, and it has been shown that the former may contribute significantly to the radiative surface flux [2], in addition to the latter.

Most boundary layers on hypersonic vehicles are turbulent, and fluctuations in temperature and species composition cause fluctuations in radiative emission $\varepsilon(T, n_s)$. Because of the nonlinear dependence of ε on its parameters, we have

$$\overline{\varepsilon(T, n_s)} \neq \varepsilon(\bar{T}, \bar{n}_s)$$

and the difference is referred to as *emission turbulence–radiation interaction* (TRI), where an overbar indicates a mean quantity.

TRI is a well-known phenomenon studied primarily in the combustion community. It is well recognized today that in the field of combustion TRI can more than double emission, leading to sharply increased radiative heat loads. See the reviews by Faeth et al. [3] and Modest [4], for example. However, the equivalent information is not yet known for hypersonic turbulent boundary layers. So far, there are very few studies of TRI for hypersonic flows. The existing Reynolds-averaged Navier–Stokes (RANS) calculations for hypersonic flows have neglected the interrelationship between radiation and turbulence, and the error introduced by such a simplification is largely uncertain.

Direct numerical simulations (DNSs) provide a vast amount of accurate data that can be used to analyze the interrelationship between turbulence and various fundamental processes. For example, Martín and Candler [5,6], Martín [7], and Duan and Martín [8] performed DNS coupled with finite rate chemistry to study turbulence–chemistry interaction in hypersonic turbulent boundary layers under typical hypersonic conditions. Wu et al. [9] and Deshmukh et al. [10] conducted DNS coupled with high-fidelity radiative transfer equation solvers to isolate and quantify the individual contributions of emission and absorption TRI for premixed and nonpremixed combustion systems, respectively. Roger et al. [11] analyzed the role of the small-scales of turbulence on thermal radiation based on the DNS data for a nonisothermal turbulent plane jet. Analyses for the interrelationship between turbulence and radiation in hypersonic boundary layers have not been performed and is the target of the present investigation.

In the current paper, we conduct DNS to assess the influence of emission TRI on radiative emission, using conditions typical of an Orion Crew Exploration Vehicle (CEV) during reentry. The effects of emission TRI will be analyzed by first using an uncoupled DNS field, which neglects the backward influence of emission on the flow and then by using DNS with emission coupled to the DNS solver.

The paper is structured as follows. The governing equations, constitutive and relations are introduced in Sec. II. The calculation of the radiative emission is introduced in Sec. III. The nondimensional governing parameter for estimating emission TRI is given in Sec. IV. Flow conditions for DNS are given in Sec. V. Numerical methods, and initial and boundary conditions, are given in Sec. VI. Results are given in Sec. VII. Finally, conclusions are given in Sec. VIII.

II. Governing Equations

The governing equations, constitutive relations and numerical method for simulation of chemically reacting flow are described in detail in Duan and Martín [12]. Therefore, only a cursory description is given here.

The equations describing the unsteady motion of a reacting fluid are given by the species mass, mass-averaged momentum, and total energy conservation equations, which, neglecting thermal nonequilibrium, are

$$\begin{aligned}
&\frac{\partial \rho_s}{\partial t} + \frac{\partial}{\partial x_j}(\rho_s u_j + J_{sj}) = w_s \\
&\frac{\partial \rho u_i}{\partial t} + \frac{\partial}{\partial x_j}(\rho u_i u_j + p\delta_{ij} - \sigma_{ij}) = 0 \\
&\frac{\partial E}{\partial t} + \frac{\partial}{\partial x_j}\left((E + p)u_j - u_i\sigma_{ij} + q_j + \sum_s J_{sj}h_s\right) = 0
\end{aligned} \tag{1}$$

When thermal radiation is included, the heat flux q_j in the total energy equation is the sum of conductive heat flux q_{Cj} and radiative heat flux q_{Rj}. The details of the calculation of the radiative heat flux is introduced in Sec. III.

The thermodynamic properties of high-temperature air species for evaluating total energy E and internal energy e_s are computed by NASA Lewis curve fits [13]. Mixture transport properties μ and κ for evaluating stress tensor σ_{ij} and conductive heat flux q_{Cj} are calculated using the Gupta et al. [14] and Yos [15] mixing rule. Fick's diffusion model with unity Lewis number is used for calculating species diffusion flux J_{sj}. An 11-species air-reaction mechanism [16] is used for gas-phase reactions. The constitutive relations and chemical mechanism are consistent with those used by NASA in the DPLR code to compute Orion entry mean flow solutions.

III. Radiative Emission Calculations

Radiative emission within the turbulent boundary layer is characterized by the emission coefficient, which at thermodynamic nonequilibrium may be approximated as a function of four temperatures (T, T_r, T_v, and T_e for translation, rotation, vibration, and electrons, respectively) and the number densities of the radiating species n_s (assumed to be N, O, N_2^+, NO, O_2, N_2, and e for Earth reentry). Within the boundary layer the gas states are close to thermodynamic equilibrium, and the local emission coefficient normalized by radiating species number density simplifies to

$$\varepsilon^*_{s\lambda} = \kappa^*_{s\lambda}(T, n_s) I_{b\lambda}(T) \tag{2}$$

If only total emission is of interest, Eq. (2) may be summed over all species and integrated over the entire spectrum and directions, or rather, by summing over all individual line strengths [17]:

$$\begin{aligned}
\varepsilon &= 4\pi \sum_s n_s \int_0^\infty \varepsilon^*_{s\lambda}\, \mathrm{d}\lambda = 4\pi \sum_s n_s \int_0^\infty \kappa^*_{s\lambda} I_{b\lambda}\, \mathrm{d}\lambda \\
&= 4\pi \sum_s n_s \sum_i \kappa^*_{s\lambda_i} I_{b\lambda_i}
\end{aligned} \tag{3}$$

where

$$\kappa^*_{s\lambda_i} = g_U B_{UL} \frac{h}{\lambda_i}\left(\frac{N_L}{n_s} - \frac{N_U}{n_s}\right) \tag{4}$$

To compute spectral emission coefficients for radiating species, a precise model to calculate the electronic excited state population, N_U and N_L in Eq. (4), of radiating gas species is required. We used the quasi-steady-state approximation of Park [16] to model the electronic energy state populations for the atomic radiating species and a Boltzmann distribution for molecular species.

In the current analysis, only emission is considered (the medium is optically thin). The radiative heat flux is calculated by

$$\nabla \cdot \mathbf{q}_R = \varepsilon \tag{5}$$

where the total emission ε is computed using Eq. (3).

IV. Governing Parameters for Emission TRI

The difference between $\overline{\varepsilon(T, n_s)}$ and $\varepsilon(\bar{T}, \bar{n}_s)$ is a measure of emission TRI intensity and indicates how total emission gets

Table 1 Dimensional boundary layer edge and wall parameters for large-eddy simulations

Parameter	Value
M_δ	0.153
ρ_δ, kg/m^3	0.011
T_δ, K	9614
T_w, K	2607
Re_θ	68
Re_τ	388
$Re_{\delta 2}$	189
θ, mm	4.0
H	0.1
δ, mm	24.0

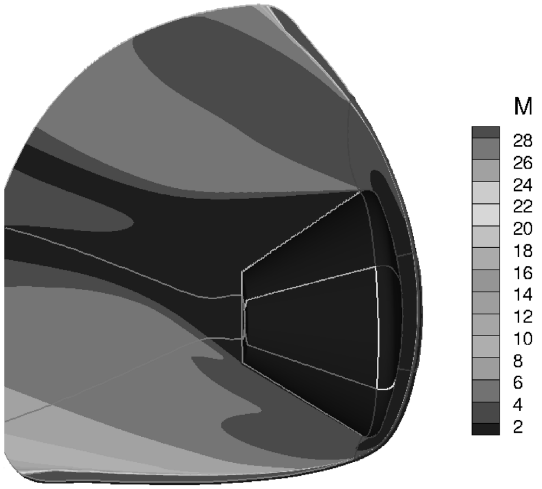

Fig. 1 Mach number contours for a three-dimensional DPLR solution of Orion at peak-heating reentry conditions.

augmented due to turbulent fluctuation. To further predict how such augmentation effects influence the overall turbulent flowfield, we propose the nondimensional parameters based on the flow governing equations.

Thermal emission acts as a sink of energy in the total energy equation. To estimate the heat loss due to emission TRI, we introduce interaction relative heat loss $\overline{\Delta h}^I$, which is defined as

$$\overline{\Delta h}^I \equiv \frac{(\overline{\varepsilon(T,n_s)} - \varepsilon(\bar{T},\bar{n}_s))\tau_t}{\sum_{i=1}^{ns} \bar{\rho}_i(h_i(\bar{T}) + \frac{1}{2}\tilde{u}_k\tilde{u}_k)} \tag{6}$$

where τ_t is some characteristic turbulence time scale, the choice of which may be large-eddy turnover time δ/U_δ, or q/ϵ, which is the time scale for energy-containing eddies, and $\overline{\varepsilon(T,n_s)} - \varepsilon(\bar{T},\bar{n}_s)$ is included to measure the intensity of emission TRI.

The interaction relative heat loss is the ratio of enhanced heat loss due to emission TRI during the characteristic flow time to the total flow enthalpy, and provides a measure of the relative importance of the heat loss effects by emission TRI. If the magnitude of $\overline{\Delta h}^I$ is close to or larger than unity, a significant change in flowfield by emission TRI is expected.

V. Flow Conditions

We consider the boundary layer for Orion CEV, which enters the Earth's atmosphere at 9.5 km/s, altitude of 53 km, and angle of 18°. These conditions represent Earth entry, at peak-heating. Table 1 shows the boundary-layer edge conditions and wall parameters for the DNS domain, which are established by extracting them from a larger domain finite volume RANS calculation. The RANS solution is obtained (as a courtesy from NASA Ames) using a well-established NASA computational fluid dynamics solver, DPLR [18], and considers chemical reaction processes of 11 species: N, O, N^+, O^+, N_2, O_2, NO, N_2^+, O_2^+, NO^+, and e. Figure 1 shows the entire computational domain for the RANS finite volume solution, and Figs. 2a and 2b show the identified DNS subdomain. The DNS

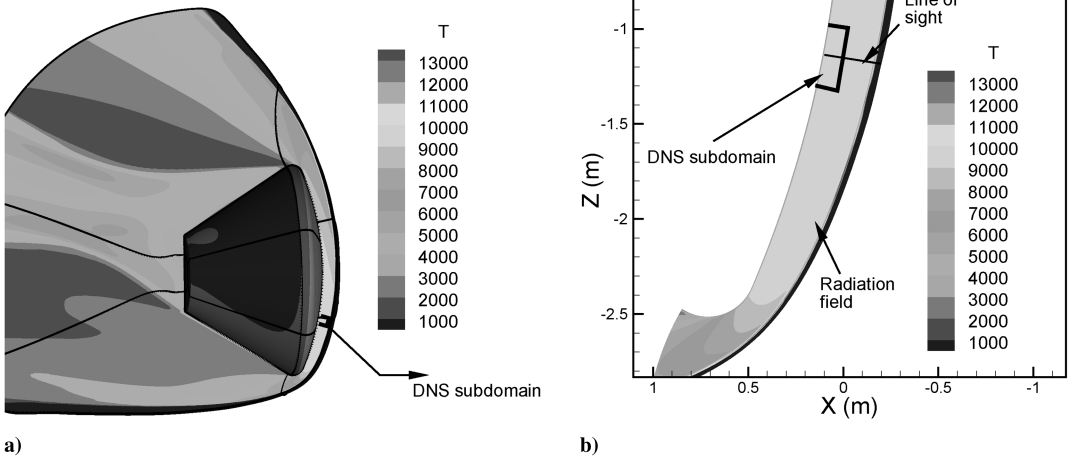

a) b)

Fig. 2 DNS subdomain from CEV solution.

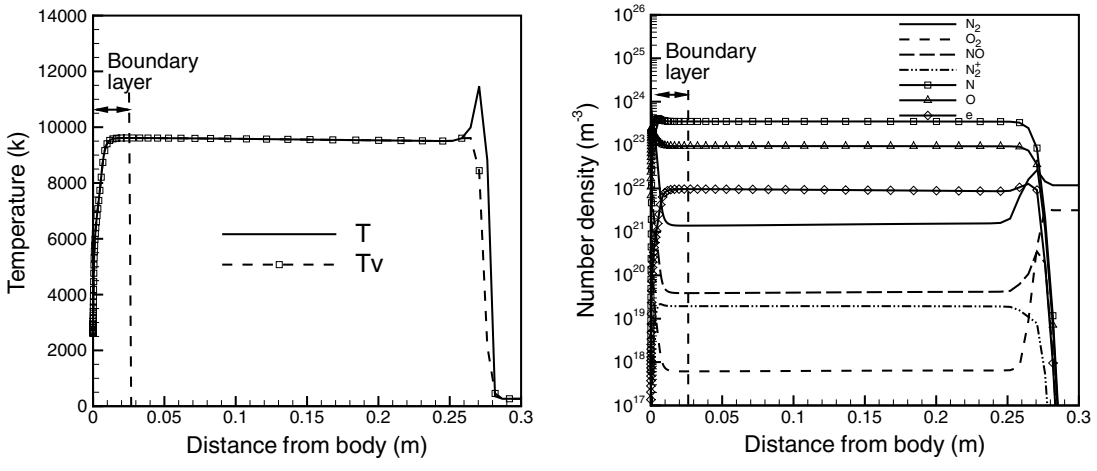

a) b)

Fig. 3 Temperatures and number densities along the line of sight indicated in Fig. 2b from the DPLR RANS solution.

Table 2 Grid resolution and domain size for the initial DNS field

Parameter	Value
L_x/δ	9.3
L_y/δ	1.9
L_z/δ	15.2
Δx^+	7.8
Δy^+	2.9
z_2^+	0.31
α	1.061
N_x	55
N_y	60
N_z	60

subdomain lies toward the front of the craft, where the temperature and electron number density are high and radiation is strong, as shown in Fig. 3. The temperatures as well as number densities of radiating species (N, O, N_2^+, NO, O_2, and N_2 for Earth reentry) along the line of sight are indicated in Fig. 2b. For the presently estimated Orion peak-heating conditions, it was found that the strong turbulence is limited to the aft region of the spacecraft, where radiation is weak. Therefore, to investigate a worst-case scenario, a relatively large turbulence level (maximum $\sqrt{q}/u_\tau \approx 2.2$ or $\sqrt{q}/U_\delta \approx 7\%$), typical of that in the attached boundary-layer aft region, is prescribed to the selected DNS subdomain. The analysis then represents a combination of strong turbulence together with strongest radiation to present a worst-case scenario for an Earth entry of Orion, or of a hypothetical case of a larger vehicle, to determine whether or not TRI may be of importance. The use of one temperature model for the DNS subdomain is justified, since the vibrational temperature at the selected conditions is equal to the translational temperature throughout the boundary layer, as shown in Fig. 3a.

Table 3 DNS cases

Cases	Radiative heat flux
I	$\nabla \cdot \mathbf{q}_R = 0$
II	$\nabla \cdot \mathbf{q}_R = \varepsilon(T, n_s)$
III	$\nabla \cdot \mathbf{q}_R = \varepsilon(\bar{T}, \bar{n}_s)$

VI. Numerical Method: Initial and Boundary Conditions

Regarding the numerical method, the spatial derivatives are computed using a fourth-order-accurate, bandwidth-optimized weighted essentially nonoscillatory scheme [19]. To perform the numerical integration, we use a third-order-accurate low-storage Runge–Kutta method by Williamson [20]. The viscous terms are computed using a fourth-order-accurate central scheme. A description of the code and its validation are given are given in DNS mode in Martín [21] and Duan and Martín [12].

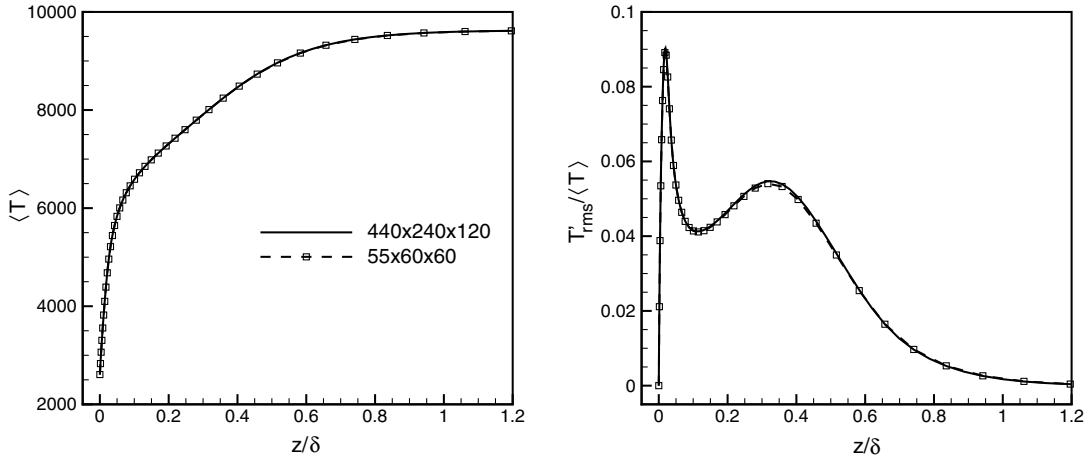

a) b)

Fig. 4 Grid-convergence study varying $N_x \times N_y \times N_z$ for DNS case I.

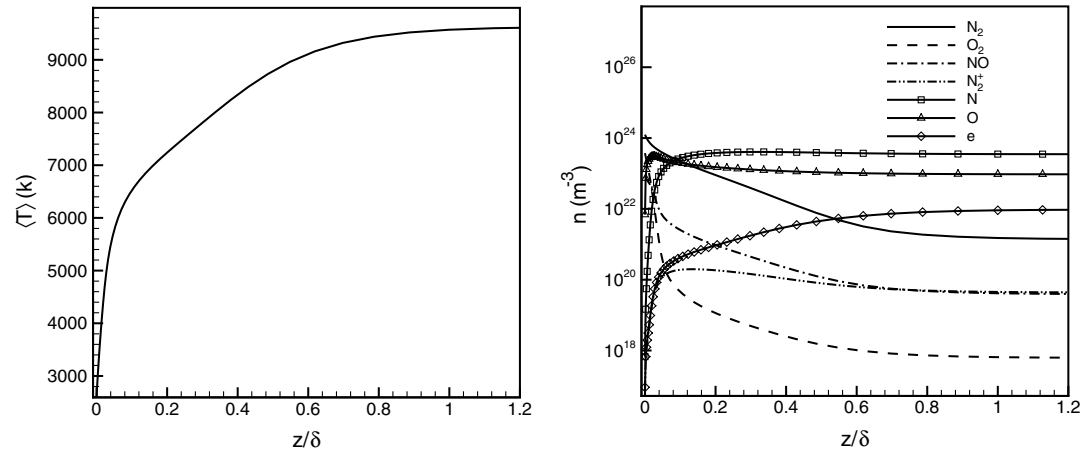

a) b)

Fig. 5 Mean temperature and species number densities for DNS case I.

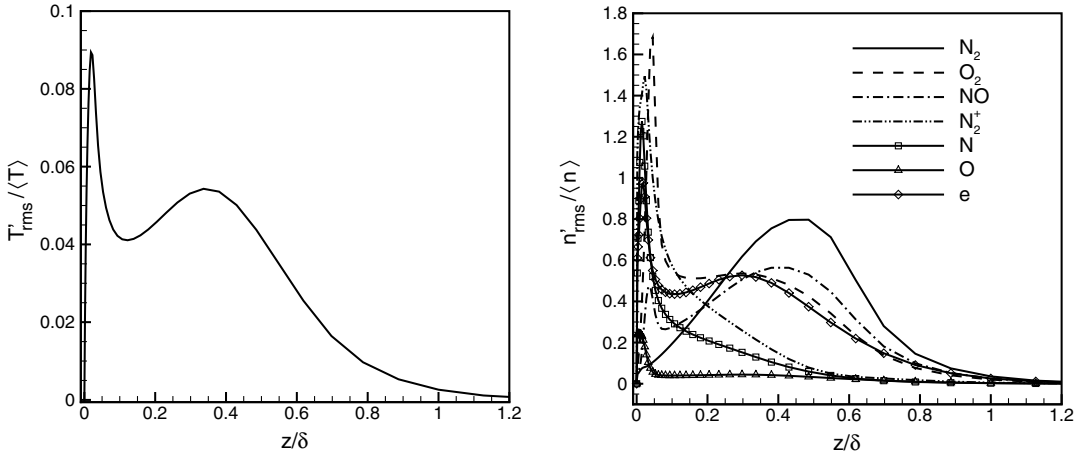

a) b)

Fig. 6 Fluctuations in temperature and species number densities relative to local mean for DNS case I.

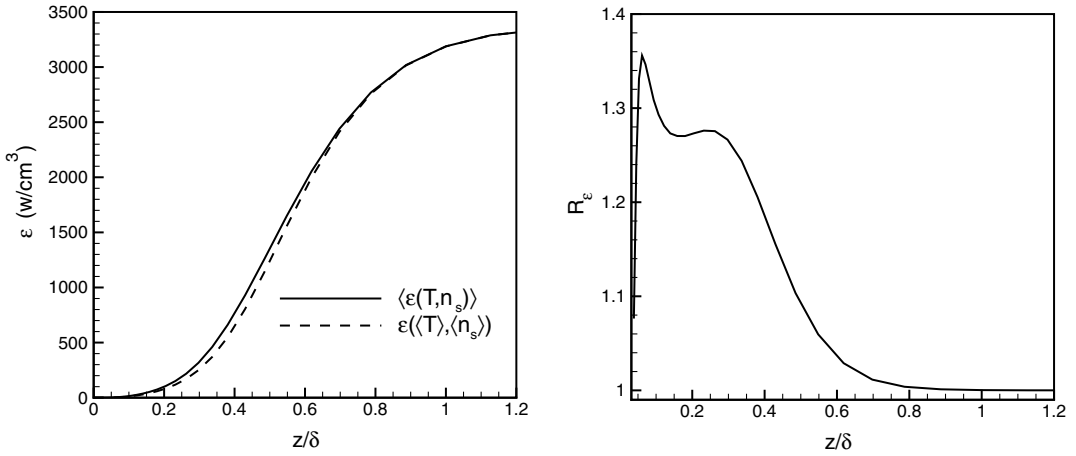

a) b)

Fig. 7 Total emissions for case I.

The initial DNS flowfield is obtained by first extracting the mean profiles from the RANS calculation at the location indicated in Fig. 2 and then superimposing the fluctuating field. The fluctuating field is obtained by transforming that of an incompressible turbulent boundary-layer DNS using well-established scaling laws. The details of this initialization technique are introduced by Martín [21]. The domain size ($L_x \times L_y \times L_z$), the grid size ($\Delta x \times \Delta y \times \Delta z$), and the number of grid points ($N_x \times N_y \times N_z$) for the initial DNS field are given in Table 2. We take the streamwise, spanwise, and wall-normal directions to be x, y, and z, respectively. Uniform grid spacings are used in the streamwise and spanwise directions with constant Δx^+ and Δy^+, where the superscript + indicates scaling with inner, or wall, values. Geometric stretching is used in the wall-normal direction, with $z_k = z_2(\alpha^{k-1} - 1)/(\alpha - 1)$.

The sensitivity of the solution to the grid size can be assessed by grid-convergence study, as shown in Figs. 4a and 4b, which plot the mean temperature and rms temperature, respectively, with different numbers of grid points for case I (shown in Table 3). All the corresponding curves collapse to within 2%, indicating the insensitivity of the results to the grid sizes. Similarly, the sensitivity of the solution to the time step has been assessed by comparing the simulations with various Courant–Friedrichs–Lewy numbers. It should be noted that the resolution requirements for very cold wall simulations, as it is the case here, are not as stringent as those for simulations with adiabatic walls [22].

Nonslip wall boundary conditions are used for the three velocity components. The wall temperature is prescribed and kept isothermal. An equilibrium catalytic boundary condition is used for species; i.e., species go to equilibrium state at the given wall temperature. The flow conditions on the top boundary are fixed edge conditions, which are extracted from the CEV RANS calculation. Periodic boundary conditions have been used in the streamwise and spanwise directions.

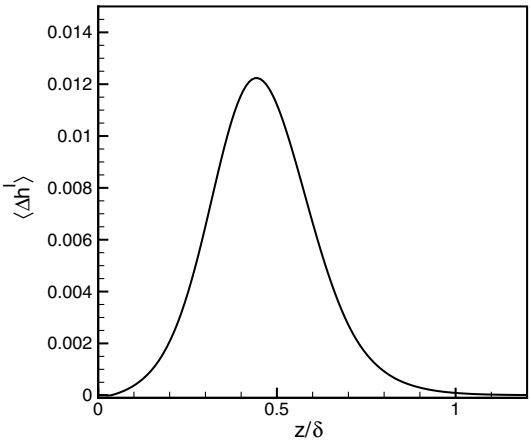

Fig. 8 Interaction relative heat loss $\overline{\Delta h^l}$ across the boundary layer for case I.

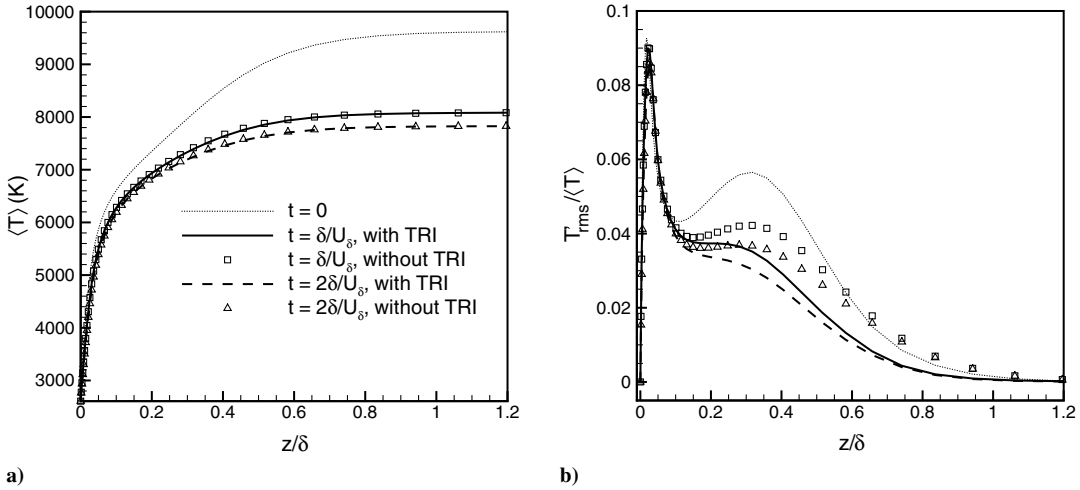

a) b)

Fig. 9 Time evolution of a) mean temperature and b) temperature fluctuations for case II (with emission TRI) and case III (without emission TRI).

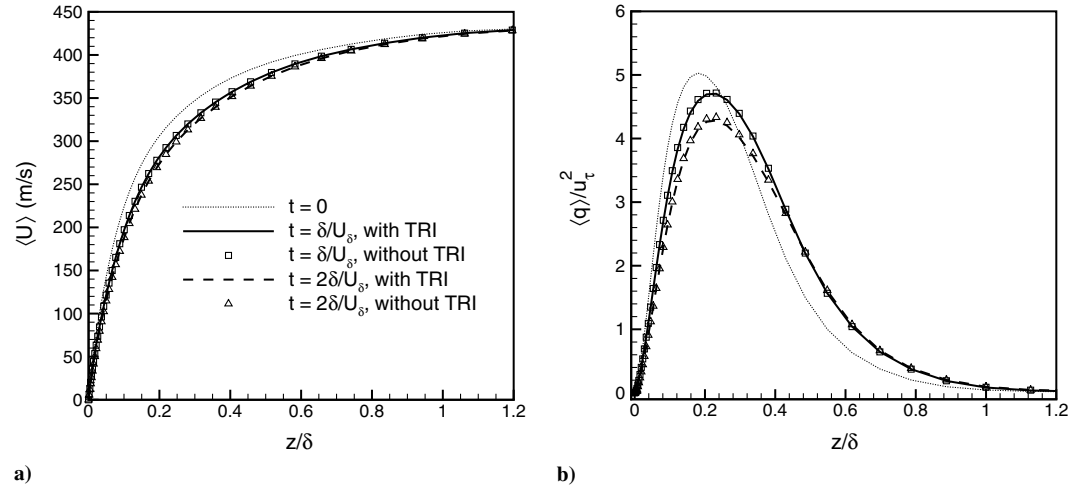

a) b)

Fig. 10 Time evolution of a) mean streamwise velocity and b) turbulent kinetic energy for case II (with emission TRI) and case III (without emission TRI).

Averages are computed over streamwise and spanwise directions for each field, then an ensemble average is calculated over fields spanning around one nondimensional time unit. The time is nondimensionalized by δ/u_τ. The average of f over the x and y directions will be denoted by $\bar{f}$, or $\langle f \rangle$, and fluctuations about this mean will be denoted by f'.

VII. Results

To investigate the effects of emission TRI, we perform three different DNS cases, as listed in Table 3. In case I, emission is uncoupled to the flow with $\nabla \cdot \mathbf{q}_R = 0$. In case II, emission is fully coupled to the turbulent flowfield. In case III, emission is included,

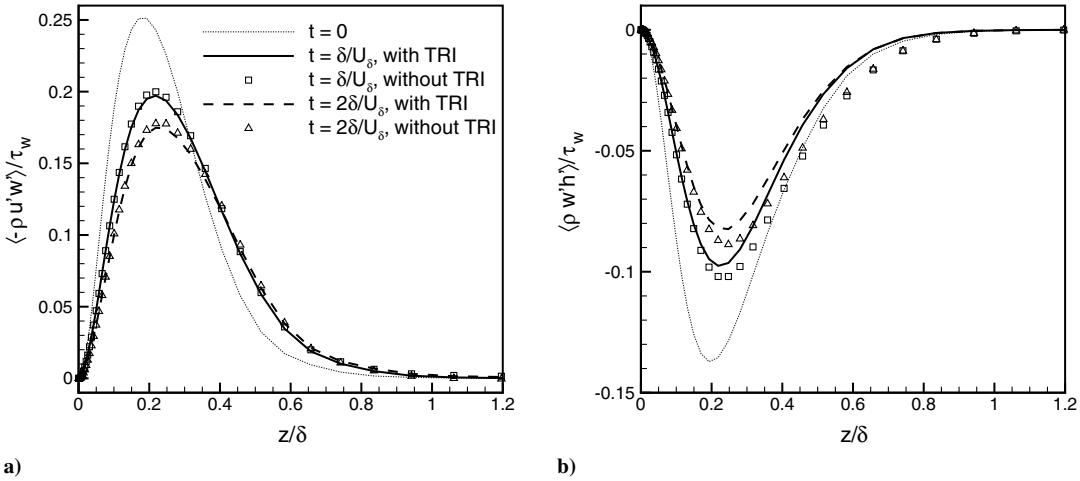

a) b)

Fig. 11 Time evolution of a) Reynolds shear stress $-\overline{\rho u' w'}/\tau_w$ and b) turbulent heat flux $\overline{\rho w' h'}/\bar{\rho}_w u_\tau \bar{h}_w$ for case II (with emission TRI) and case III (without emission TRI).

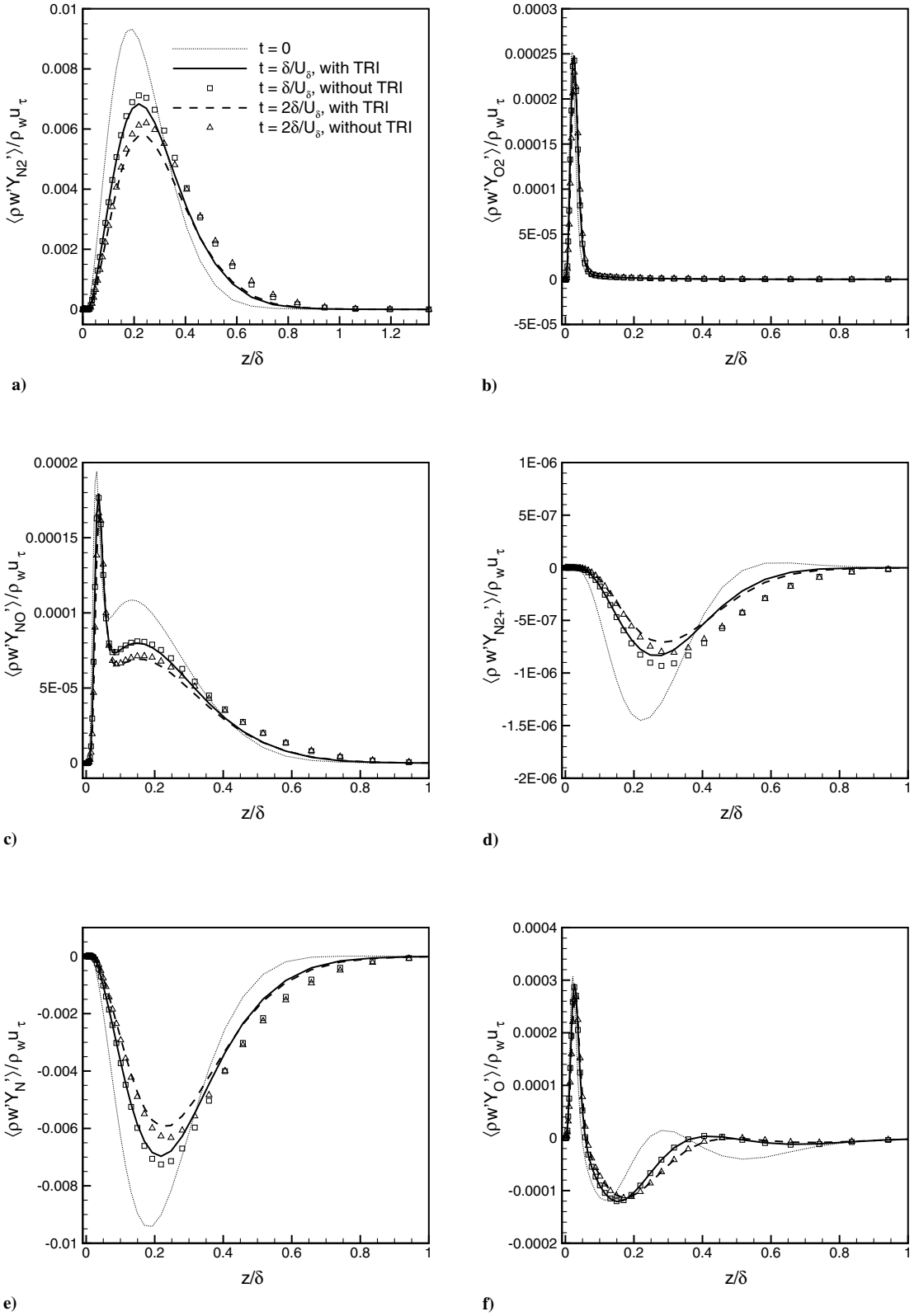

Fig. 12 Time evolution of turbulent mass flux $\overline{\rho w' Y_s'}/\bar{\rho}_w u_\tau$ for case II (with emission TRI) and case III (without emission TRI): a) N_2, b) O_2, c) NO, d) N_2^+, e) N, and f) O.

but calculated based only on the mean flow quantities, excluding the interaction between turbulence and emission.

A. Case I Study

In case I study, DNS is conducted with the same thermal and chemical models as DPLR solution, where radiation has been neglected. As a result, the DNS solution has similar mean temperature and species number densities (Fig. 5) as the DPLR solution at the same location. Figure 6 plots normalized fluctuations in temperature and number densities across the boundary layer. It is shown that the maximum temperature fluctuation relative to the mean is about 9%, and the maximum fluctuations in species number densities range from 20% for O to 60% for O_2.

To investigate how total emissions get augmented due to turbulent fluctuations, Fig. 7a plots $\overline{\varepsilon(T, n_s)}$ and $\varepsilon(\bar{T}, \bar{n}_s)$, and Fig. 7b plots the ratio between the two $R_\varepsilon \equiv \overline{\varepsilon(T, n_s)}/\varepsilon(\bar{T}, \bar{n}_s)$. While the total emission gets amplified by turbulence fluctuations with maximum relative difference of more than 30%, as shown in Fig. 7b, most amplification happens close to the wall, where $\varepsilon(\bar{T}, \bar{n}_s)$ itself is small, due to the relative low temperature. The absolute difference between $\overline{\varepsilon(T, n_s)}$ and $\varepsilon(\bar{T}, \bar{n}_s)$ is small all through the boundary layer, as it is shown in Fig. 7a.

To predict the effect of emission TRI on the turbulence flowfield, Fig. 8 plots the interaction relative heat loss. It is shown that $\overline{\Delta h'}$ is at least two orders smaller than unity, indicating that the enhanced heat loss due to emission TRI has little influence on the turbulent flowfield.

B. Cases II and III Studies

We further analyze the influence of emission TRI on the turbulent flowfield by coupling radiative emission to the flow solver in two different approaches: one with emission TRI (case II) and one without emission TRI (case III), as shown in Table 3. The initial turbulent field is in a statistically stationary state when emission is not active ($\nabla \mathbf{q}_R = 0$). After the emission term is turned on, the nonzero radiative heat flux due solely to emission results in a nonstationary state in which the flow cools down. We perform DNS and monitor the evolution of the turbulent quantities as they depart from their original state. The effects of emission TRI on the turbulent flowfield can be isolated by comparing results between cases II and III at different time instants after emission has been turned on.

At the instant emission is turned on, we set $t = 0$. Turbulence statistics are collected at $t = \frac{\delta}{U_\delta}$ and $t = 2(\delta/U_\delta)$, respectively. Figure 9a plots the mean temperature at $t = 0, \delta/U_\delta$, and $2(\delta/U_\delta)$ for all the cases. For both cases II and III, the mean temperature decreases significantly when radiation is introduced. The magnitude of temperature fluctuations also decreases, as it is shown in Fig. 9b. There is nearly no difference in mean temperature with and without TRI, consistent with the small values of $\overline{\Delta h'}$, as shown in Fig. 8. However, the emission TRI results in further decrease in the magnitude of temperature fluctuations, relative to the results without TRI, with relative differences being as large as 20% at $t = \delta/U_\delta$.

In terms of the velocity field, Figs. 10a and 10b plot the time evolution of the mean streamwise temperature and turbulent kinetic energy, respectively, for all cases. It is shown that emission reduces turbulence in the flow. As a result of energy loss in the flow, the mean velocity profile becomes less full and the magnitude of TKE decreases after radiation is introduced. In addition, both the mean velocity and TKE are nearly the same for cases II and III, indicating that the effects of emission TRI on the velocity field are negligible.

To demonstrate the influence of emission TRI on turbulent transport of momentum, heat and mass, Figs. 11a, 11b, and 12 plot normalized Reynolds shear stress, turbulent heat flux and turbulent mass fluxes for radiating species, respectively, for cases II and III. The sizable decreases in Reynolds shear stress and turbulent heat and mass fluxes further indicate the flow is less turbulent after emission is introduced. The small differences between cases with and without emission TRI indicate insignificant influence of emission TRI on the turbulent transport terms and is consistent with the small values of $\overline{\Delta h'}$.

The influence of emission TRI on total emission can be shown by Figs. 13a and 13b, which plot the time evolution of total emission $\overline{\varepsilon(T, n_s)}$ and rms of total emission, respectively, for cases II and III. Similar to mean temperature and turbulent transport terms, total emission decays significantly after radiation is coupled to the flow. The difference in $\overline{\varepsilon(T, n_s)}$ between case II and case III is subtle. However, there exists significant difference in rms of total emission (as large as 40% at $t = \delta/U_\delta$).

VIII. Conclusions

Direct numerical simulations of turbulent boundary layers were conducted to study emission turbulence–radiation interaction, using conditions typical of Orion crew exploration vehicle at peak-heating during reentry. DNS fields with and without emission coupling are considered. The uncoupled results show that emission TRI only subtly increases total emission at the condition considered. When emission is coupled to the flow, the temperature decreases dramatically. In addition, the flow becomes less turbulent; the mean velocity profile becomes less full; and the turbulent kinetic energy, temperature fluctuation, and turbulent transport terms decrease significantly. The coupled results also show that emission TRI has no sizable influence on mean quantities (mean temperature, velocity, and total emission), turbulent kinetic energy, or turbulent transport terms, but has significant influence on temperature fluctuations and total emission fluctuations. The nondimensional governing-parameter interaction relative heat loss provides a good metric for estimating the influence of emission TRI on the turbulence flowfields.

The insignificant influence of emission TRI on the turbulent flow dynamics for hypersonic boundary layers is different from what have been found for many combustion flows, as described in Sec. I. The possible reason for the difference is that in typical Earth reentry conditions, the atomic species such as N and O are the strongest radiators [23]. The generation of these radiating species requires the reaction of air, which happens at significantly higher temperatures ($T > 2500$ K) than those for typical combustion applications. The significantly higher flow enthalpy required to initialize the air reactions overwhelms the enhanced heat loss due to emission TRI, as

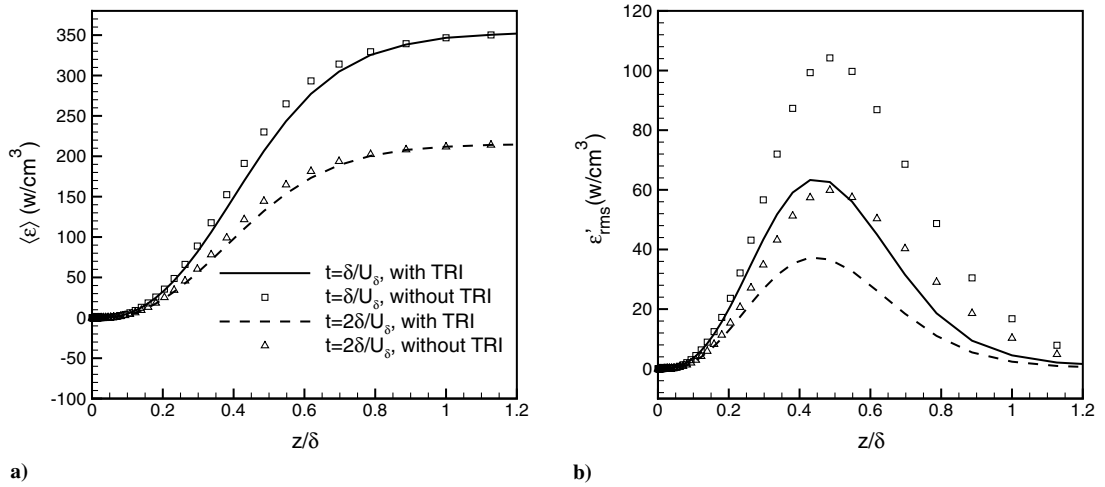

a) b)

Fig. 13 Time evolution of a) mean and b) rms of total emission for case II (with emission TRI) and case III (without emission TRI).

indicated in Fig. 8. However, given the limited number of flow conditions explored, further investigation may be necessary to confirm this argument.

Acknowledgments

This work is sponsored by NASA Constellation University Institutes Project grant NCC3-989. We thank Peter Gnoffo for insightful discussions and the Space Technology Division in NASA Ames Research Center for providing Reynolds-averaged Navier–Stokes solutions under flow conditions representative of Crew Exploration Vehicles.

References

[1] Whiting, E. E., and Park, C., "Radiative Heating at the Stagnation Point of the AFE Vehicle," NASA TM 102829, 1990.

[2] Feldick, A. M., Duan, L., Modest, M. F., Martín, M. P., and Levin, D. A., "Influence of Interactions Between Turbulence and Radiation on Transmissivities in Hypersonic Turbulent Boundary Layers," 48th AIAA Aerospace Sciences Meeting, AIAA Paper 2010-1185, Orlando, FL, Jan. 2010.

[3] Faeth, G. M., Gore, J. P., Chuech, S. G., and Jeng, S. M., "Radiation from Turbulent Diffusion Flames," *Annual Review of Numerical Fluid Mechanics and Heat Transfer*, Vol. 2, 1989, pp. 1–38.

[4] Modest, M. F., "Multiscale Modeling of Turbulence, Radiation and Combustion Interactions in Turbulent Flames," *International Journal of Multiscale Computational Engineering*, Vol. 3, No. 1, 2005, pp. 85–106.
doi:10.1615/IntJMultCompEng.v3.i1.70

[5] Martín, M., and Candler, G., "DNS of Mach 4 Boundary Layer with Chemical Reactions," AIAA Paper 2000-0399, 2000.

[6] Martín, M., and Candler, G., "Temperature Fluctuation Scaling in Reacting Turbulent Boundary Layers," AIAA Paper 2001-2717, 2001.

[7] Martín, M., "Exploratory Studies of Turbulence/Chemistry Interaction in Hypersonic Flows," AIAA Paper 2003-4055, 2003.

[8] Duan, L., and Martín, M. P., "Assessment of Turbulence-Chemistry Interaction in Hypersonic Turbulent Boundary Layers," *AIAA Journal*, Vol. 49, No. 1, 2011, pp. 172–184.
doi:10.2514/1.J050605

[9] Wu, Y., Haworth, D. C., Modest, M. F., and, Cuenot, B., "Direct Numerical Simulation of Turbulence/Radiation Interaction in Premixed Combustion Systems," *Proceedings of the Combustion Institute*, Vol. 30, Combustion Inst., Pittsburgh, PA, 2005, p. 639.

[10] Deshmukh, K. V., Haworth, D. C., and Modest, M. F., "Direct Numerical Simulation of Turbulence-Radiation Interactions in Homogeneous Nonpremixed Combustion Systems," *Proceedings of the Combustion Institute*, Vol. 31, Combustion Inst., Pittsburgh, PA, 2007, p. 1641.

[11] Roger, M., Coelho, P., and da Silva, C. B., "Relevance of the Subgrid-Scales for Large Eddy Simulations of Turbulence-Radiation Interactions in a Turbulent Plane Jet," *Journal of Quantitative Spectroscopy and Radiative Transfer* (to be published).

[12] Duan, L., and Martín, M., "An Effective Procedure for Testing the Validity of DNS of Wall-Bounded Turbulence Including Finite Rate Reactions," *AIAA Journal*, Vol. 47, No. 1, 2009, pp. 244–251.
doi:10.2514/1.38318

[13] Gordon, S., and McBride, B., "Computer Program for Calculation of Complex Chemical Equilibrium Compositions and Applications," NASA Ref. Publ. 1311, 1994.

[14] Gupta, R., Yos, J., Thompson, R., and Lee, K., "A Review of Reaction Rates and Thermodynamic and Transport Properties for 11-Species Air Model for Chemical and Thermal Non-Equilibrium Calculations to 30000 K," NASA RP-1232, 1990.

[15] Yos, J., "Transport Properties of Nitrogen, Hydrogen, Oxygen, and Air to 30,000 K," Avco. Corp., TR AD-TM-63-7, Wilmington, MA, 1963.

[16] Park, C., "Non-Equilibrium Hypersonic Aerodynamics," Wiley, New York, 1990.

[17] Sohn, I., Bansal, A., Levin, D. A., and Modest, M. F., "Advanced Radiation Calculations of Hypersonic Reentry Flows Using Efficient Databasing Schemes," *Journal of Thermophysics and Heat Transfer*, Vol. 24, No. 3, July–Sept. 2010, pp. 623–637; also AIAA Paper 2008-4019.

[18] Wright, M. J., White, T., and Mangini, N., "Data Parallel Line Relaxation (DPLR) Code User Manual," NASA Ames Research Center, TM 2009-215388, Moffett Field, CA, 2009.

[19] Taylor, E., Wu, M., and Martín, M., "Optimization of Nonlinear Error Sources for Weighted Non-Oscillatory Methods in Direct Numerical Simulations of Compressible Turbulence," *Journal of Computational Physics*, Vol. 223, 2007, pp. 384–397.
doi:10.1016/j.jcp.2006.09.010

[20] Williamson, J., "Low-Storage Runge–Kutta Schemes," *Journal of Computational Physics*, Vol. 35, No. 1, 1980, pp. 48–56.
doi:10.1016/0021-9991(80)90033-9

[21] Martín, M., "DNS of Hypersonic Turbulent Boundary Layers. Part I: Initialization and Comparison with Experiments," *Journal of Fluid Mechanics*, Vol. 570, 2007, pp. 347–364.
doi:10.1017/S0022112006003107

[22] Duan, L., Beekman, I., and Martín, M., "Direct Numerical Simulation of Hypersonic Turbulent Boundary Layers. Part II: Effect of Wall Temperature," *Journal of Fluid Mechanics*, Vol. 655, 2010, pp. 419–445.
doi:10.1017/S0022112010000959

[23] Ozawa, T., Wang, A., Modest, M. F., and Levin, D. A., "Particle Methods for Simulating Atomic Radiation in Hypersonic Reentry Flows," *Rarefied Gas Dynamics*, Vol. 1084, American Inst. of Physics, Melville, NY, 2008, pp. 748–753.

T. Jackson
Associate Editor